Mitigation of Losses from Hydrodynamic Mixing in a Hydrogen Bromine Laminar Flow Battery

by

Laura M. Gilson

B.S. Mechanical Engineering
Massachusetts Institute of Technology, 2013

SUBMITTED TO THE DEPARTMENT OF MECHANICAL ENGINEERING IN PARTIAL FULFILLMENT OF THE REQUIREMENTS FOR THE DEGREE OF

MASTER OF SCIENCE IN MECHANICAL ENGINEERING
AT THE
MASSACHUSETTS INSTITUTE OF TECHNOLOGY

FEBRUARY 2016

Signature of Author..... Signature redacted
Department of Mechanical Engineering
January 15, 2016

Certified by..... Signature redacted .....
Cullen R. Buie
Associate Professor of Mechanical Engineering
Thesis Supervisor

Accepted by..... Signature redacted .....
Rohan Abeyaratne
Professor of Mechanical Engineering
Chairman, Committee on Graduate Students

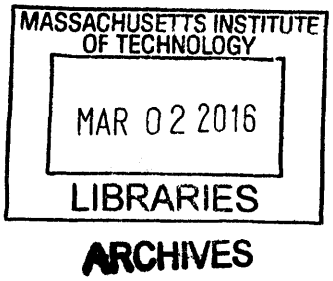

ARCHIVES

Mitigation of Losses from Hydrodynamic Mixing in a Hydrogen Bromine Laminar Flow Battery

by

Laura M. Gilson

Submitted to the Department of Mechanical Engineering on January 15, 2016 in Partial Fulfillment of the Requirements for the Degree of Master of Science in Mechanical Engineering

ABSTRACT

The hydrogen bromine laminar flow battery is a promising technology for grid-scale energy storage. It dispenses with the expensive membrane used in traditional flow batteries, instead using laminar flow to maintain the separation of fluid streams. It also takes advantage of powerful, inexpensive chemical reactants. However, mixing between the fluid streams within the battery reduces its single-pass performance and cyclability. Conditions at the inlet junction where oxidant and electrolyte streams come together are thought to influence mixing. This work investigates the relationship between fluid flow at the inlet junction, mixing, and battery performance. Matching electrolyte- and oxidant-stream flow rates or velocities is predicted to cause less mixing than employing hydrodynamic focusing of the oxidant stream. When hydrodynamic focusing is used in channels with heights on the order 500 μm or less, numerical simulations show recirculating flows at the inlet junction and experimental results show a decrease in limiting current. However, for matching inlet velocities or flow rates experimental results show limiting current consistent with predictions that assume no mixing. This result shows a path forward achieving higher power density in the hydrogen bromine laminar flow battery by prioritizing symmetry of the inlet flow conditions as the channel height is decreased.

Thesis Supervisor: Cullen R. Buie
Title: Associate Professor of Mechanical Engineering

Acknowledgements

I would like to thank my advisors, Professor Cullen Buie and Professor Martin Bazant, for their guidance and support.

I am grateful to Dr. William Braff, for his pioneering work on the hydrogen bromine laminar flow battery, to Dr. Matthew Suss, who introduced me to the experimental work on the battery, and to Kameron Conforti, for his continuing contributions to the project. I would also like to thank other labmates past and present: Naga Neehar Dingari, Dr. Paulo Garcia, Zhifei Ge, Andrew Jones III, Dr. Youngsoo Joung, Dr. Jeffrey Moran, Alisha Schor, and Qianru Wang in the Laboratory for Energy and Microsystems Innovation, and Dr. Peng Bai, Dr. Yossi Cohen, Joey Gu, Dr. Jihyung Han, Fan He, Edwin Khoo, Yamini Krishnan, Nancy Lu, Dr. Mohammed Mirzadeh, Dr. Elisha Rejovitsky, Carlos Sauer, Sven Schlumpberger, Raymond Smith, Juhyun Song, and Tingtao Zhou in the Bazant group. Thanks also to Truong Cai for his assistance with machining and experiments, and to MIT's UROP program, for making his work possible.

Thanks to Matthew Houston, Emily Gilson, Linda Gilson, and Tom Gilson for their encouragement, inspiration, and support leading up to and throughout this project.

This material is based upon work supported by the National Science Foundation Graduate Research Fellowship under Grant No. 1122374.

Table of Contents

List of Figures

List of Tables

Chapter 1

Introduction

1.1 Energy storage

1.1.1 The need for grid-scale storage

The development of better, cheaper energy storage technology is poised to have far-reaching impact. Today's electric vehicles, for example, are limited by existing storage technology: extending their driving range depends on batteries becoming more energy dense.[1] On a larger scale, the electrical power grid is turning to storage as a means of improving the grid's efficiency and incorporating renewable energy resources at a large scale. Further development of inexpensive, scalable, and geographically flexible energy storage methods will accelerate this change.[2]

The power grid stands to benefit from incorporating storage in several ways. First, storage allows better utilization of the most efficient generation equipment. In the United States, most energy is produced and delivered to consumers with no intermediate storage available, so the generation capacity that must be available to provide power during times of peak demand sits idle during periods of low demand.[3] With storage, energy produced by the most efficient equipment available during times of low demand can offset the need for extra generation capacity during times of peak demand, increasing the efficiency of the entire grid.

Additionally, storage makes it practical to incorporate intermittent renewable energy resources as a large fraction of the grid's power generation base. For example, renewables such as wind and solar come with no assurance that power will be reliable or even available when users demand it. However, with sufficient storage, even a grid that is highly dependent on intermittent resources can provide reliable power.[4] Storage is an attractive solution to the problem of intermittency if renewables are to provide more than a token fraction of the energy in a power grid.

1.1.2 The state of grid-scale energy storage

For the reasons discussed above, grid-scale energy storage is an area of increasing interest. Several storage technologies are mature but limited in where they may be deployed, while others promise greater flexibility, but remain in development.

Two successfully implemented energy storage techniques, pumped hydroelectric and compressed air, are limited by their need for a particular geography. Pumped hydroelectric facilities on the scale of a few thousand megawatts typically have efficiencies around 70-80%, but this method requires sites that can provide two large water reservoirs at different elevations.[5] Compressed air energy storage has also been implemented commercially. It relies on well-studied technology (pumps and compressors) for power conversion, and stores compressed air in geologic formations such as caverns and aquifers.[6] Both methods are limited to specific kinds of landscapes, though they are otherwise well suited to bulk energy storage.[6] Though some mechanical energy storage technologies are appropriate for long-term storage applications, additional solutions will likely be needed to meet the demand for storage where these methods are not practical. Electrochemical energy storage is an alternative that is not subject to these geographical constraints.

1.1.3 Electrochemical energy storage

Electrochemical energy storage methods include batteries, which convert electrical to chemical energy for storage via electrochemical reactions, and supercapacitors, which store energy in the electric double layer that forms adjacent to a charged surface. In addition to requiring no particular geography, electrochemical energy storage typically has a much faster response time than other methods.[2] In particular, redox batteries, which convert between stored chemical energy and useful electrical energy via pairs of redox reactions, have been proposed for grid-scale energy storage.

Batteries are ubiquitous in mobile power devices, but stationary batteries for grid-scale power are a new market opportunity. Batteries engineered for different applications typically differ in chemistry and architecture. Rechargeable lithium ion batteries, which typically power laptops and cellular telephones, have a high energy density, and so are the best option when battery weight is a concern.[1] Grid-scale storage, on the other hand, is often stationary and has a less pressing need for high energy density.

Battery performance is specified using several figures of merit. Cycle life refers to the number of charge-discharge cycles that a battery can undergo without significant loss in capacity, or energy that can be stored.[1] Several measures of efficiency are commonly specified as well. Voltage efficiency is the ratio of voltage during discharge to voltage during charging at the same current magnitude. Coulombic efficiency is the ratio of the charge extracted from the battery during discharge to the charge passed into the cell during charging. The product of voltage efficiency and coulombic efficiency, energy efficiency, is the fraction of the energy used to charge the cell that can be extracted.[7]

1.1.4 Redox flow batteries

In a battery, the electrochemical reactions that convert electrical to chemical energy occur at the electrodes, which conduct electrons from or to the external circuit, and which are in contact with the electrolyte, through which ions are transported across the cell. In a conventional battery, electrode material is a product or reactant in those reactions, which means that chemical energy is stored in the electrode. In contrast, in a redox flow battery, the products and reactants remain dissolved in the electrolyte, which is pumped through the cell. The two electrolyte streams, known as the anolyte and catholyte streams, each contain the products and reactants of one of the pair of redox reactions. These streams are typically separated by an ion exchange membrane. In this way, a flow battery is similar to a fuel cell, but, unlike fuel cell reactions, flow battery reactions are easily reversible, so the batteries are rechargeable.[8]

Because the redox products remain dissolved in the electrolyte, flow battery capacity is determined by the size of the tanks that hold the electrolyte. Power, on the other hand, depends on the size of the electrode. A basic advantage of the redox flow battery is that capacity and power are uncoupled, allowing flexibility in system design.[4] Other advantages of redox flow batteries over other rechargeable batteries include a longer lifespan due to the lack of phase-change, the absence of harmful effects if the battery is fully discharged, the flexibility to charge and discharge the battery at different voltages, and the simplicity of maintenance and monitoring of state of charge.[7] Disadvantages include a more complicated system required to run the battery, including pumps with moving parts.[9]

A broad range of flow battery chemistries has been proposed and demonstrated.[4] Early prototypes used all-vanadium chemistry. This chemistry avoids some problems associated with

crossover and mixing: any vanadium ion that crosses the membrane self-discharges harmlessly. However, the all-vanadium battery's power is limited by the solubility of vanadium.[4] In the first decade of the 2000s, a number of vanadium redox flow batteries ranging from 1 kW to eventually 1 MW scale were built and demonstrated in Japan, South Africa, China, and the United States. However, due to the batteries' expense, they have yet to emerge as a truly competitive option.[10] Several companies are working to commercialize vanadium flow battery technology, but affordability remains a challenge.[11]

1.2 Hydrogen bromine laminar flow battery

1.2.1 Laminar flow batteries

In a flow battery, the ion-exchange membrane functions to allow the transport of select ions between the anolyte and catholyte streams, while preventing the transport of other species and bulk mixing between the streams. Keeping the anolyte and catholyte streams separate is important, because their separation provides the driving force for the electrochemical reaction from which electrical energy can be harvested. Membranes, while very good at separating, add expense and ion transport losses to a cell. Eliminating the membrane may be beneficial if there is a less costly way to prevent the anolyte and catholyte streams from mixing with each other.

Microfluidics researchers have pointed out that in a low-Reynolds number laminar flow, convective mixing is suppressed. Thus in a microfluidic fuel cell operating at a low Reynolds number, the anolyte and catholyte streams flow in parallel with very little mixing or crossover, even without a membrane.[12] These fuel cells and flow batteries that rely upon low-Reynolds number flow to maintain separation of anolyte and catholyte streams are called membraneless or laminar flow fuel cells or flow batteries. Figure 1-1 illustrates the difference between membrane-equipped and membraneless flow batteries. Sometimes, as shown in Figure 1-1, a third electrolyte stream helps to maintain the separation of the anolyte and catholyte stream. This is the case in the hydrogen bromine laminar flow battery that is studied in this work.

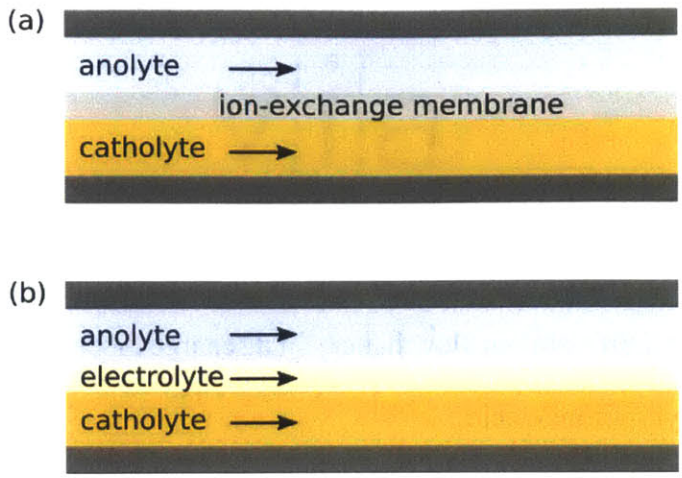

Figure 1-1: (a) Traditional flow battery versus (b) membraneless flow battery.

1.2.2 Hydrogen bromine chemistry

Hydrogen bromine chemistry for flow batteries has been explored for several decades. In 1980, a hydrogen bromine flow battery was demonstrated with low kinetic losses and an efficiency of over 70%[13], and NASA also investigated the hydrogen bromine battery in the 1980s.[14] In recent years, a hydrogen bromine flow battery being developed at Lawrence Berkeley National Laboratory has demonstrated a peak power density of 1.46 W/cm^2 [15] and energy efficiency of around 70% during long-term cycling experiments, in which over 600 cycles were demonstrated.[16] Unfortunately, the performance of their cell is limited by the resistance of the membrane, which increases with increasing electrolyte concentration due to dehydration.[16] The membrane limitation makes the hydrogen bromine flow battery a good candidate for a membraneless design.[17]

The relatively low cost of the both hydrogen and bromine is a large factor in the attractiveness of hydrogen-bromine systems. Compared to vanadium, bromine is inexpensive (about a quarter the price of vanadium in 2014, on a per-mole basis[18]) and abundant: global vanadium resources are somewhere over 63 million metric tons; in contrast, an estimated 1 billion metric tons of bromine are to be found in the Dead Sea alone.[18] In addition to being relatively inexpensive, this redox couple typically exhibits fast kinetics, meaning that below limiting current, losses are primarily ohmic and determined by the cell architecture.[19]

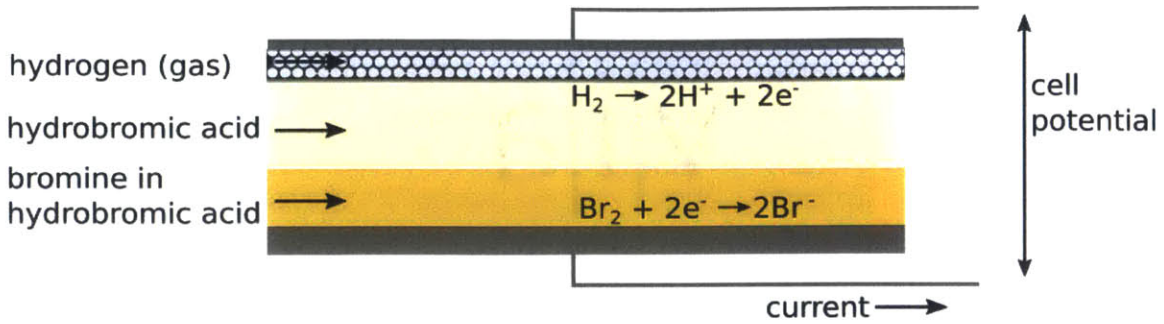

Figure 1-2: Hydrogen bromine laminar flow battery in discharge mode. Electrochemical reactions at the electrode surface drive electrical current to the external circuit, as hydrogen and bromine react to form hydrobromic acid.

There are some drawbacks to working with hydrogen-bromine chemistry. The hydrogen storage system does contribute significantly to cost.[20] Hydrobromic acid and bromine are corrosive, which limits material compatibility. Additionally, working with hydrogen, hydrobromic acid, and bromine presents hazards that must be managed. Nevertheless, the quick kinetics and cheap reactants make hydrogen bromine chemistry a competitive candidate for grid scale storage.

Figure 1-2 illustrates the hydrogen bromine laminar flow battery with the electrochemical reactions shown in discharge mode. In this membraneless design, the hydrobromic acid electrolyte stream separates the hydrogen gas stream from the bromine stream, which is also referred to as the oxidant stream. This battery is the focus of the flow simulations and polarization curve experiments presented in this work.

1.2.3 Mixing in the hydrogen bromine laminar flow battery

As in any membraneless flow battery, preventing mixing between streams is extremely important. Mixing reduces the battery's state of charge without releasing power to the external circuit. In the hydrogen bromine flow battery, mixing reduces the concentration of bromine available to react at the cathode during discharge. It also exposes platinum catalyst on the anode to bromide, which is suspected to poison the electrode.[14]

In previous work with the hydrogen bromine laminar flow battery, the battery achieved the limiting current predicted by a boundary-layer analysis at a channel height of 800 μm,[19] but not at a channel height of 600 μm.[21] Further studies suggested that mixing at the junction where the bromine inlet channel joins the electrolyte inlet channel plays a role. In two-dimensional

numerical simulations of fluid flow and transport of dilute species, the smaller channel height exhibited a recirculating flow pattern within the oxidant stream at the inlet that enhanced diffusion between the electrolyte and oxidant stream.[22] These experiments and simulations employed a 10:1 flow electrolyte-to-oxidant flow rate ratio, in order to hydrodynamically focus the oxidant stream against the electrode. The advantages and disadvantages of this and other inlet flow conditions are discussed further in Chapter 2.

1.3 Organization

This work is centered on the questions of how the flow at the inlet junction in the hydrogen bromine laminar flow battery influences mixing between the bromine and hydrobromic acid streams, and how such mixing affects battery performance. It is organized as follows:

Chapter 2 provides an overview of the fluid mechanics, transport, and electrochemical reactions occurring in the laminar flow battery. Chapter 3 presents the results from numerical simulations for the fluid flow at the laminar flow battery inlet, demonstrating that the asymmetric inlet flow conditions associated with hydrodynamic focusing of the oxidant are especially conducive to recirculating flow in the inlet in the 2-dimensional case. Chapter 4 discusses the design and construction of the hydrogen bromine laminar flow battery prototype. Chapter 5 presents experimental results from that prototype showing the dependence of the battery's limiting current on inlet flow conditions and channel height, which show signs of mixing in the same conditions that demonstrate the strongest recirculating flow at the inlet in the two-dimensional numerical simulations. Chapter 6 discusses conclusions and future work.

Chapter 2

Fluid Flow and Electrochemistry in the Laminar Flow Battery

2.1 Introduction

This work is primarily concerned with optimizing the single-pass performance of the hydrogen bromine flow battery. However, the ultimate goal is to evaluate its appropriateness as a stationary battery, and these experiments should be considered in the context of their ultimate applicability to battery cycling.

Mixing can be a particularly important problem for membraneless flow batteries. In a flow battery, active material (in this case bromine) can be lost from its own stream to another (in this case the electrolyte) due to crossover. A small amount of crossover is expected due to diffusion, especially with a membraneless cell. However, crossover is made much worse by transverse flow across the cell. This can happen in a membraneless cell if the fluid flow is not carefully managed.

Limiting mixing of fluid streams in membraneless flow batteries is necessary for achieving optimal performance. State of charge describes a battery's location on the spectrum between fully charged and fully discharged states. In a flow battery, the state of charge is related to the concentration of reactants circulating through the battery. As reactants are consumed, the state of charge drops; as they are replenished, the state of charge is restored. Mixing reduces the concentration of reactants, and thus reduces the battery's state of charge without actually producing current.

The electrochemical performance of the hydrogen bromine laminar flow battery depends on its fluid mechanics in two primary ways. First, losses associated with transport reduce the voltage the cell can provide at finite currents. As the current through the battery increases, the cell reaches a limiting current, due to transport limitations. The transport of species in the cell is through the moving fluid, and so depends on the fluid flow. Additionally, fluid flow that is favorable to mixing between the electrolyte and oxidant streams will reduce the oxidant

concentration adjacent to the electrode, thereby reducing the cell's open circuit potential in accordance with the Nernst equation described in Section 2.2.1.

This chapter discusses the ways in which fluid flow and electrochemistry interact in the hydrogen bromine flow battery. It provides background for predicting how the limiting current in this battery will depend on channel height and for understanding flow conditions that encourage mixing.

2.2 Electrochemistry and transport in the battery

2.2.1 Nernst: concentration affects open circuit potential

The electrochemical potential at which the anolyte and catholyte stream are in electrochemical equilibrium is also known as the open circuit potential; it is the potential at which no current flows into or out of the cell.

This potential depends upon the concentration of the redox products and reactants in the anolyte and catholyte streams according to the Nernst equation:

$$\Delta\phi_{cell}^{eq} - \Delta\phi_{cell}^{0} = -\frac{RT}{zF}\ln\left(\frac{\Pi_{\text{products}}(a^{\nu})_{\text{products}}}{\Pi_{\text{reactants}}(a^{\nu})_{\text{reactants}}}\right) \tag{1}$$

where $\Delta\phi_{cell}^{eq}$ is the equilibrium cell potential (open circuit potential), $\Delta\phi_{cell}^{0}$ is the standard cell potential, R is the universal gas constant, T is the temperature, z is the number of electrons transferred per reaction, F is Faraday's constant, a's are the activities of the products and reactants, and ν's are the stoichiometric coefficients of the products and reactants. Assuming dilute solutions, activities are approximately given by concentrations. The net reaction is

$$H_2 + Br_2 \rightarrow 2HBr \tag{2}$$

with a standard cell potential[23] of 1.087 V and with two electrons transferred per reaction, as shown in Figure 1-2.

It may be seen from (1) that as the concentration of bromine (a reactant) decreases, the cell's open circuit potential also decreases. In cases where the fluid flow induces mixing upstream of the channel, as it would if there were mixing at the inlet junction, the concentration of bromine at the electrode is reduced, as illustrated in Figure 2-1. This leads to a reduction in the

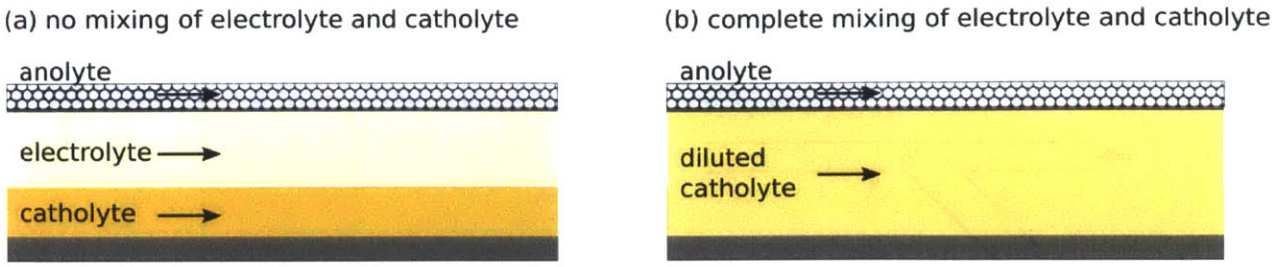

Figure 2-1: Extremes of mixing. (a) the fully unmixed case, where the bulk catholyte remains at its inlet concentration over the length of the cell. (b) the fully mixed case, where complete mixing has occurred upstream of the main channel, e.g. at the inlet, and the bulk catholyte has been fully diluted by the electrolyte stream.

open circuit potential. This is observed in some of the polarization curves presented in Chapter 5, where it is associated with mixing.

It can also be seen from the Nernst equation that as the concentration of bromine approaches zero, the cell potential approaches $-\infty$. This is the mechanism by which the formation of a bromine depletion layer at electrode causes a limiting current, the value of which depends on transport in the cell.

2.2.2 Limiting current behavior

Inside the cell, the transport of reactants to the electrodes must balance the current through the external circuit, according to the stoichiometry of the electrochemical reactions occurring at the electrodes. When the concentration of a reactant drops to zero at the electrode, the current becomes limited to the rate at which that reactant can be transported to the electrode.

Braff et al.[19] investigated the mass transfer limitation in the hydrogen bromine laminar flow battery using a boundary layer analysis in the limiting case in which the concentration of bromine is zero everywhere along the electrode, illustrated in Figure 2-2. The analysis assumes a parabolic Poiseuille flow profile, which is expected for channels whose inter-electrode height is much smaller than the channel width. The combination of this flow profile and this concentration boundary condition produces a Leveque concentration boundary layer.

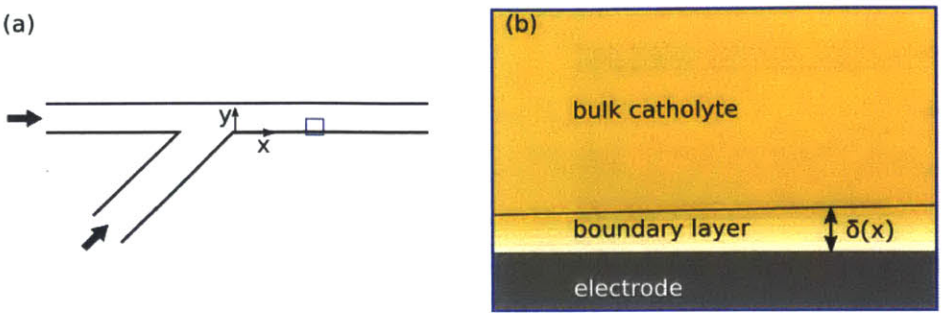

Figure 2-2: Boundary layer formation at limiting current. (a) shows the location of (b), illustrating a boundary layer of depleted oxidant forming along the cathode during discharge at limiting current.

One result of this analysis is an expression for the length-averaged limiting current density due to the depletion of bromine at the cathode during battery discharging:[19]

$$\bar{J}_{\lim} = \frac{3zD_{Br2}Fc^{0}_{Br2}}{h}\frac{\left(\frac{9Pe}{4\beta}\right)^{1/3}}{\Gamma\left(1/3\right)} \tag{3}$$

The Péclet number is $Pe = \frac{Uh}{D} = \frac{\nu}{D}Re$, the length-height aspect ratio is $\beta = \frac{L}{h}$, the bulk concentration of bromine far from the wall is c^{0}_{Br2}, the diffusivity of bromine is D_{Br2}, and the channel height is h. For the same Reynolds number Re, the limiting current should scale as $h^{-2/3}$. This expression provides the predicted limiting current at as a function of channel height. This result is compared with experimental results in Chapter 5.

In this expression, limiting current depends linearly on the bulk concentration. If that changes, for example due to mixing between the oxidant and electrolyte channel, the limiting current density will decrease proportionally to the concentration.

2.2.3 Bulk electrolyte resistance

Channel height also affects the rate at which cell potential changes with increasing current density. In the limiting case of small currents, ($\bar{J} \ll \overline{J_{lim}}$), the boundary layer is small and provides very little resistance to transport. Because the hydrogen bromine battery typically has very fast kinetics,[24] the primary losses in the battery at low concentrations are expected to

come from bulk electrolyte resistance and any additional hardware resistance. The bulk electrolyte resistance is due to the conductivity of the electrolyte and the cell's geometry:

$$R_b = \frac{h}{\sigma w L} \tag{4}$$

Here σ is the conductivity of the electrolyte, which is a function of electrolyte concentration. Bulk electrolyte resistance depends linearly on channel height, so it is advantageous to reduce the channel height to improve power output and round-trip efficiency.

2.2.4 Net effect on battery performance

At zero current, the total cell potential is equal to the open circuit potential. As the magnitude of the current is increased, during discharge, the potential drops. Some of the drop in cell potential is due to the bulk electrolyte resistance, which depends linearly on the current. There is an additional drop in potential due to the formation of the boundary layer, whose dependence on current is more complicated.[19]

2.2.5 A note on mixing within vs. across streams

Mixing within the anolyte or catholyte streams, which has been achieved through such means as patterned electrodes,[25] is a desirable feature in planar electrode flow cells. This is distinct from the mixing between the oxidant and electrolyte streams, which this work is trying to understand and avoid. In the hydrogen bromine laminar flow battery's architecture, the role of the electrolyte stream is to keep the bromine from reaching the hydrogen electrode. Mixing between the electrolyte and oxidant streams allows bromine to reach the hydrogen electrode, contributing to degradation of cell materials, loss of single-pass performance due to dilution of the catholyte, and loss of cycling performance due to the loss of active material.

2.2.6 Bounds on the effects of mixing

Leaving a discussion of how mixing might occur at the inlet until Section 2.3, it can already be seen that a reduction in the concentration of bromine will affect the performance of the hydrogen bromine laminar flow battery. This occurs in two ways: a decrease in bromine concentration reduces both the open circuit potential, via the Nernst equation, and the limiting current, via the boundary layer limiting current.

A lower bound on the limiting current as affected by mixing, can be given by assuming the case in which the electrolyte and oxidant stream mix completely. Evaluating the limiting current assuming the bulk bromine concentration is the concentration of the bromine stream upstream of the inlet gives an upper bound, while evaluating the limiting current assuming the bromine and electrolyte streams have fully mixed gives a lower bound. These correspond to the unmixed and fully mixed cases in Figure 2-1. Partial mixing may result in a limiting current somewhere between these bounds. The unmixed predicted limiting current and the fully mixed predicted limiting current are plotted alongside the experimental limiting current data in Chapter 5.

2.3 Flow

In the hydrogen bromine laminar flow battery, the interface between the electrolyte and the oxidant streams is supposed to be protected from convective mixing by low-Reynolds number flow. However, in this hydrogen bromine laminar flow battery, the Reynolds number is typically around 10. As noted with other large microfluidic devices,[26] for flow in devices with moderate Reynolds numbers, the Stokes flow assumption of negligible inertia terms in the Navier-Stokes equation is not valid.

2.3.1 Unidirectional flow in the main channel

The geometry and direction of flow in the hydrogen bromine laminar flow battery are labeled in Figure 2-3. In the main channel, inertia may be neglected, as the channel is straight and of constant cross-sectional area, and the velocity field is well described by unidirectional planar Poiseuille flow. However, this assumption is not appropriate at the inlet junction, where the oxidant flow is forced to turn a corner.

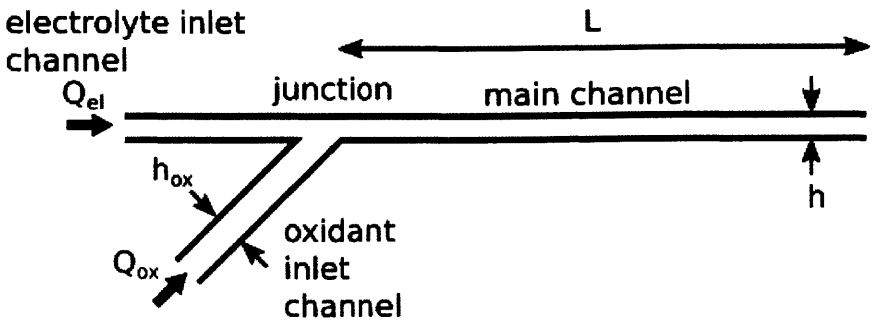

Figure 2-3: Geometry and flow in the hydrogen bromine laminar flow battery. The main channel is in contact with the electrodes and coincides with the active area. The electrolyte inlet channel is an extension of the main channel, with the same height h and width. The oxidant inlet channel joins the main channel at a 45° angle, and has height h_{ox}.

2.3.2 Flow at the inlet junction

Upstream of the main channel, the oxidant stream inlet channel joins the electrolyte inlet channel at a 45-degree angle. In this study, the oxidant inlet channel is always the same height (800 μm), while the electrolyte inlet channel height is always the same as the main channel height, which varies. The Reynolds number throughout this study (Re = 10) is neither very large nor very small, and the geometry at the junction is not simple, so the Navier-Stokes equation cannot be simplified to give an analytical solution for the flow profile.

2.3.3 Hydrodynamic focusing of the oxidant

All previous work with the planar-electrode hydrogen bromine flow battery used hydrodynamic focusing to focus the bromine stream against the adjacent electrode, in order to increase fuel utilization.[17] Hydrodynamic focusing is the process of introducing fluid streams into a channel at different flow rates, so that as the flow develops, the faster flow slows down and takes up a larger fraction of the width of the channel, and the slower flow speeds up and is "focused" into a small fraction of the width of the channel.

Hydrodynamic focusing has been shown to improve fuel utilization in laminar flow fuel cells.[27] Fuel utilization is important for fuel cells, because any oxidant that isn't used in a single pass is wasted. However, in a battery, each stream is recirculated, so fuel utilization is less of a concern. The importance of mixing between streams, on the other hand, is magnified, because of the associated reduction in state of charge.

It is not immediately obvious to what extent hydrodynamic focusing should affect mixing at the inlet junction. Hydrodynamic focusing at intermediate Reynolds numbers has been shown

to produce a curved interface due to inertial effects, especially when the higher inertia sheath flow is introduced through a side channel and so must bend.[28] Previous simulations of the flow in the inlet of the hydrogen bromine laminar flow battery using hydrodynamic focusing showed the formation of a recirculating flow in the bromine inlet stream, but did not compare that case to cases without focusing.[22]

For batteries, the usefulness of hydrodynamic focusing of the oxidant stream is marginal. A more important goal in setting oxidant and inlet flow rates for a given Reynolds number is to minimize mixing.

2.3.4 Designing inlet and flow rates for low mixing

Experimental studies and numerical modeling of mixing in T-junction micromixers show that for symmetric geometries and equal inlet flow rates, the onset of mixing downstream of the junction occurs at a Reynolds number of over 100.[29–31] Figure 2-4 illustrates a common T-junction geometry for mixing studies. The Reynolds number in the hydrogen bromine laminar flow battery is typically of order 10. The T-mixer studies suggest that if the battery were redesigned as a T-junction, with equal electrolyte and oxidant flow rates, it would be possible to maintain an undisturbed interface along the length of the channel at the Reynolds number of interest. In the T-junction studies, the geometric symmetry means that equal inlet flow rates imply equal inlet velocities. In the hydrogen bromine laminar flow battery, the inlet channels are typically not the same height, so either the flow rates or the velocities can be matched, but not both.

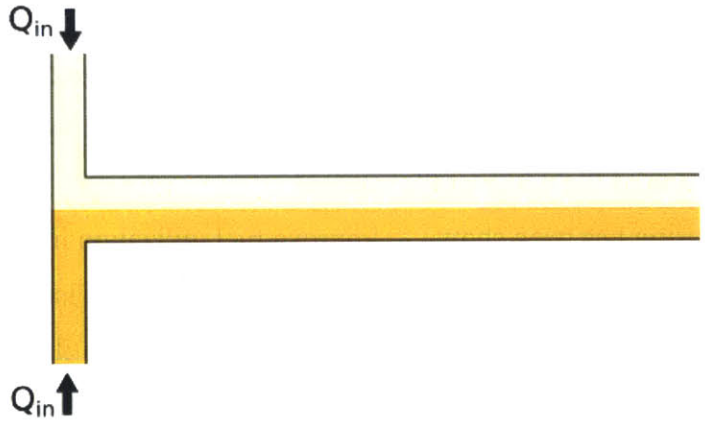

Figure 2-4: Schematic of two streams coming together in a symmetric T-junction with equal inlet flow rates, exhibiting no mixing.

Considering the hydrogen bromine laminar flow battery, a T-junction is not the most practical geometry to build. The present architecture (Figure 2-3) allows the electrolyte inlet channel to be an extension of the main channel, cut from the same gaskets. This simplifies cell fabrication, but causes asymmetry in the angle at which the electrolyte and oxidant flows are introduced. This geometric asymmetry is exacerbated when the main channel height is decreased while the oxidant inlet channel, which is cut into the electrode, stays the same.

A hypothesis explored in this work is that, even with these geometric asymmetries, matching either the flow rate or the velocity of the two inlet streams will prevent mixing. Furthermore, it is expected that a reduction in mixing will lead to higher limiting currents as channel heights decrease, as predicted by the boundary layer analysis. Matching velocities is a good candidate for reducing mixing, because the inertia of each inlet stream is directly dependent on the velocity. However, the location of the interface between the oxidant and the electrolyte in the main channel downstream of the junction depends more directly upon the inlet flow rates. These three conditions, hydrodynamic focusing, matched inlet flow rates, and matched inlet velocities, are examined in simulation of the flow in Chapter 3, and in experiments with the battery prototype in Chapter 5.

Chapter 3

Modeling of Inlet Flow

3.1 Introduction

Even in the simplified case of two-dimensional flow, the geometry at the junction of the oxidant and the electrolyte inlet channels is complex enough to require a numerical solution to the Navier-Stokes equations governing fluid flow. Here, numerical simulation using Comsol Multiphysics software (Comsol, Burlington, MA) was used to explore the effect of the relative magnitude of inlet flow rates on the flow at the junction for several channel heights. The results show that, in the two-dimensional case, hydrodynamic focusing conditions contribute to the formation of a recirculating flow in the inlet channel, especially when the difference in height between the main channel and inlet branch channel is large.

3.2 Flow at the inlet junction

3.2.1 Background

Previously, the idea that that the hydrogen bromine laminar flow battery's failure to achieve the predicted limiting current at a height of 600 μm was due to inertial mixing at the inlet was supported with modeling showing the presence of a recirculating vortex at the inlet.[22] In that 2-dimensional model, at low channel heights, the hydrodynamic focusing of the bromine stream occurs before the end of the junction with the bromine inlet, which remains 800 μm high in all cases. This causes the electrolyte to flow into the mouth of the bromine inlet, contributing to a recirculating flow.

3.2.2 Numerical simulation

A two-dimensional numerical simulation of the fluid flow at the inlet is presented here, carried out for a range of values of channel height, h, and flow rate ratio, r_f. The geometry of the simulated region is shown in Figure 3-1, with values for the geometric parameters and fluid properties given in Table 3-1. The flow, which is laminar with a Reynolds number of 10 in the main channel, is modeled using the Navier-Stokes equation

$$\rho \frac{D\vec{v}}{Dt} = -\nabla P + \mu \nabla^2 \vec{v} \tag{5}$$

where $\vec{v}$ is the velocity vector, P is the pressure, and ρ and μ are the fluid density and viscosity, respectively.

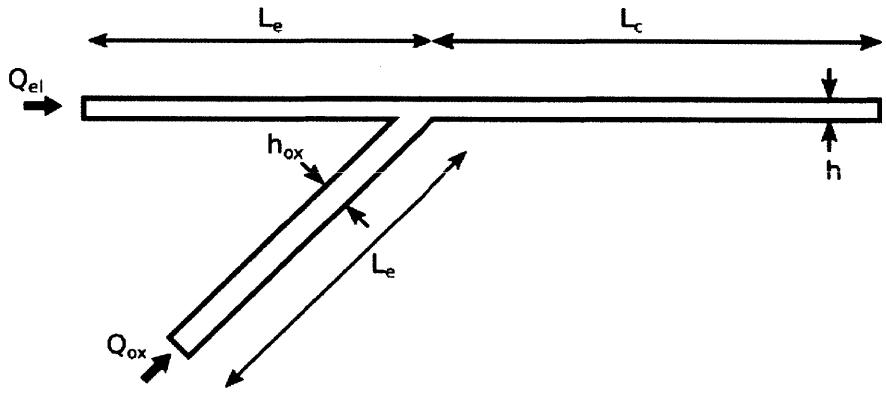

Figure 3-1: Schematic of geometry for Comsol modeling of the fluid flow at the inlet and its dependence on channel height and flow rate ratio.

Table 3-1: Parameters for fluid modeling at flow battery inlet junction.

Symbol	Value	Parameter
Re	10	Reynolds number
ρ	10^3 kg/m^3	Fluid density
μ	10^{-3}	Fluid viscosity
r_f	0.1	Flow rate ratio
h_{ox}	0.8 mm	Height of oxidant inlet channel
h	0.746 mm	Height of main channel
L_e	10 mm	Length of entrance channels
L_c	13 mm	Length of main channel
U	$\frac{\mu}{\rho h} Re$	Velocity in main channel

The boundary conditions for the fluid flow are no slip at the channel walls and zero pressure at the downstream channel exit. The inlet flow rates were also set according to the prescribed conditions.

The first case of interest was the case in which $r_f = \frac{Q_{ox}}{Q_{el}} = 0.1$, where Q_{ox} and Q_{el} are the inlet flow rates of oxidant and electrolyte, respectively. This case is the same as the hydrodynamic focusing case examined by Braff et al.[22] The second case is that of $r_f = 1$. For both, the inlet flow rates can be specified in terms of r_f.

$$Q_{el} = \frac{1}{1+r_f} \frac{\mu}{\rho} Re \tag{6}$$

$$Q_{ox} = \frac{r_f}{1+r_f} \frac{\mu}{\rho} Re$$

Holding Reynolds number constant, for each flow rate ratio, the inlet flow rates do not change as the channel height varies.

The third case of interest is the case of matched velocities, or $r_v = \frac{U_{ox}}{U_{el}} = 1$. From a mass flow balance into and out of the junction simplifies, the net flow rate out of the junction is

$$Q_{net} = Q_{el} + Q_{ox} \tag{7}$$

or

$$Uh = U_{el}h + U_{ox}h_{ox} . \tag{8}$$

The average velocities at the inlet then are

$$U_{el} = \frac{h}{h + h_{ox}r_v}\frac{\mu}{\rho h}Re \tag{9}$$

$$U_{ox} = \frac{hr_v}{h + h_{ox}r_v}\frac{\mu}{\rho h}Re .$$

The boundary conditions for flow rate are

$$Q_{el} = \frac{h}{h + h_{ox}r_v}\frac{\mu}{\rho}Re \tag{10}$$

$$Q_{ox} = \frac{hr_v}{h + h_{ox}r_v}\frac{\mu}{\rho}\frac{h_{ox}}{h}Re .$$

When r_v and Re are held constant, the flow rates do change as the channel height h is varied.

For each of these three inlet flow conditions, simulations are carried out for channel heights of 746 μm, 566 μm, 386 μm, and 206 μm. This is the same set of channel heights in the experiments described in Chapter 5. The two largest sizes are also close to the 800-μm and 600-μm channels investigated by Braff et al.[22]

3.2.3 Results of inlet flow simulations

For each of the twelve cases studied, the results of the simulations near the inlet are shown in Figure 3-2. The magnitude of the velocity is indicated by the fill color, and streamlines in the electrolyte stream are plotted in white, while streamlines in the oxidant stream are plotted in yellow.

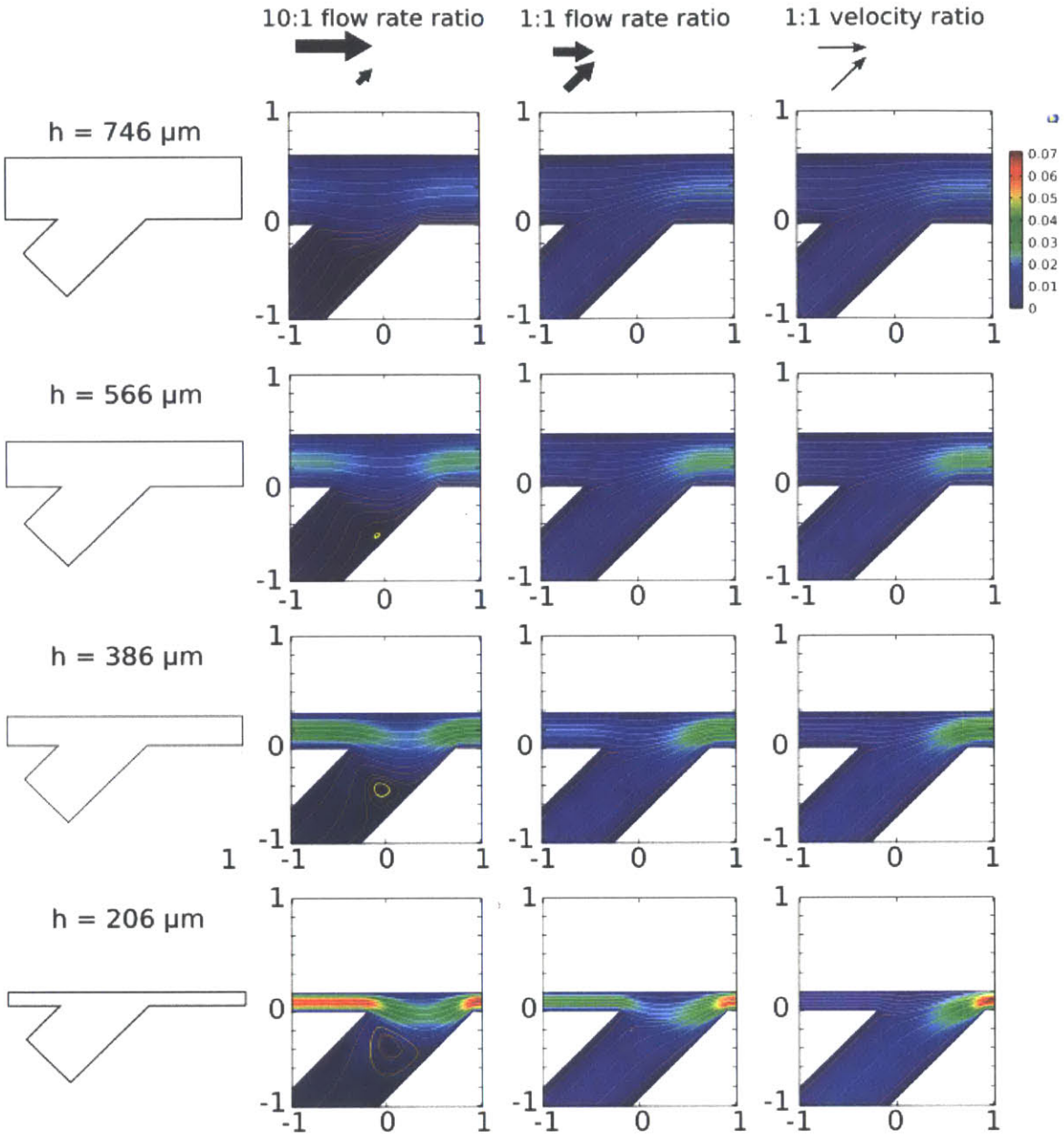

Figure 3-2: Simulated results for velocity magnitude and streamlines at the junction of oxidant and electrolyte channels. The x- and y-axis have units of millimeters. The fill color corresponds to the magnitude of the velocity, and has units of meters per second.

These results show recirculating flow in channel with height smaller than and including 566 μm, when hydrodynamic focusing is employed with a 10:1 flow rate ratio. This is consistent with what was observed by Braff et al.[22] However, in the cases of 1:1 flow rate ratio and 1:1 velocity ratio, no recirculation is seen at any of the channel heights studied. Furthermore, in the case of matched velocities, the electrolyte stream is barely even deflected into the oxidant inlet side of the junction.

3.2.4 Connection to battery performance

These results show that in a simplified two-dimensional model of the flow battery inlet, hydrodynamic focusing conditions tend to contribute to recirculating flow patterns where matched flow rates or matched velocities do not. Braff et al.'s previous work has suggested a link between this recirculation and mixing between the streams.[22]

In these simulations, matching inlet flow rates or velocities eliminates the recirculating flow associated with extreme mixing. It does not necessarily follow that applying these conditions will eliminate the mixing problem in the actual battery. The actual battery exists in three dimensional space, and may experience out-of-plane flow that enhances mixing. However, these results do identify the matched flow rate and matched velocity conditions as worth further investigation. An experimental study including these flow conditions is carried out in Chapter 5.

Chapter 4

Hydrogen Bromine Laminar Flow Battery Prototype

4.1 Introduction

The first published laminar flow fuel cell was a simple Y-channel design, molded in poly(dimethylsiloxane) (PDMS), using fabrication techniques common among microfluidic devices.[12,32] Later planar microchannels in stacked assemblies were introduced.[33] Stacked assemblies allowed the easy addition of gas diffusion electrodes, meaning reactants did not need to be in liquid solutions.[34] As gas diffusion electrodes were introduced, the logistics of handling several streams of gases and liquids led some to abandon the symmetric Y-channel design. Later, porous electrodes were introduced for liquid reactants in order to reduce transport limitations.[35] Herringbone grooves on planar electrode surfaces were also shown to increase transport and improve power.[25] Another cell used nanoporous electrodes to further enhance surface area to overcome kinetic limitations.[36]

Hydrogen-based flow batteries have drawn inspiration from hydrogen fuel cells. Hydrogen is flowed through a porous gas diffusion electrode, which interfaces with the electrolyte on one side and the current collector on the other. In a variation on this design, the anolyte or catholyte stream is a gas instead of a liquid, and flows through a porous electrode, often with a third electrolyte stream separating the two streams.[34]

Early laminar flow-based electrochemical cells were fuel cells, and were accordingly designed for high power density and fuel utilization. Flow batteries also benefit from high power density, but cyclability replaces fuel utilization as a figure of merit. The first iteration of the hydrogen bromine laminar flow battery included a porous gas diffusion electrode on the hydrogen side, a planar graphite electrode on the bromine side, and a stream of hydrobromic acid electrolyte separating the bromine from the gas diffusion electrode.[17]

Design of laminar flow batteries for cycling is gaining attention. Recently, a membraneless vanadium redox flow battery with porous electrodes demonstrated a single round-

trip cycle.[37] High cyclability was promoted by a geometry that was symmetric in the transverse and axial directions. Other recent experiments with a dual-pass membraneless fuel cell design highlight how, as membraneless flow cells approach cycling, diffusive mixing reduces performance.[38]

4.2 Cell components and their fabrication

4.2.1 Overview

The electrochemical cell of the flow battery is outlined by channel gaskets inserted between electrodes and current collectors. This assembly is clamped by two porting plates, which also provide ports through which the battery fluids can be introduced and removed. A photograph of the assembled cell is shown in Figure 4-1, and an exploded view is shown in Figure 4-2.

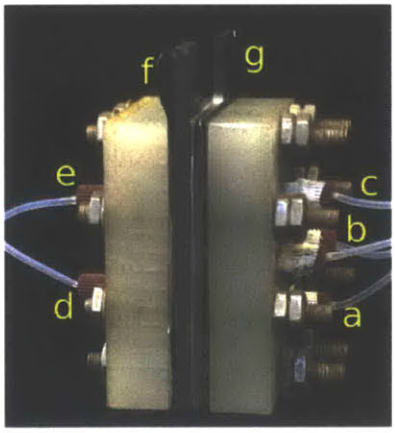

Figure 4-1: Photograph of battery prototype, including (a) hydrogen inlet, (b) electrolyte inlet (with unused port behind it), (c) hydrogen outlet, (d) oxidant inlet, (e) oxidant and electrolyte outlet, (f) connection tab for bromine electrode current collector, (g) connection tab for hydrogen electrode current collector.

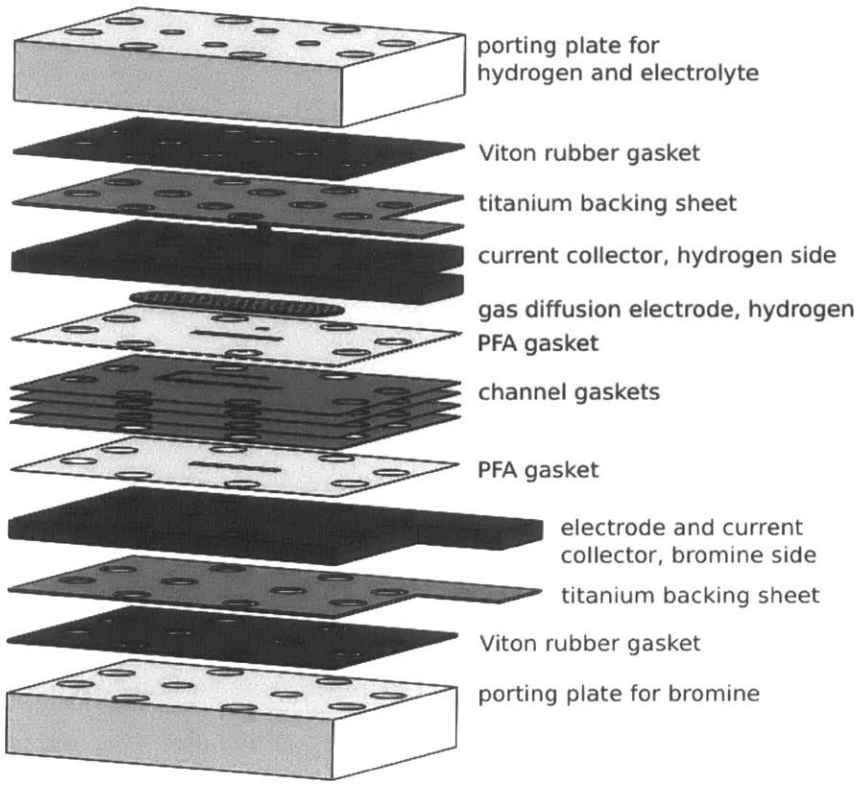

Figure 4-2: Exploded view of hydrogen bromine laminar flow battery stack assembly.

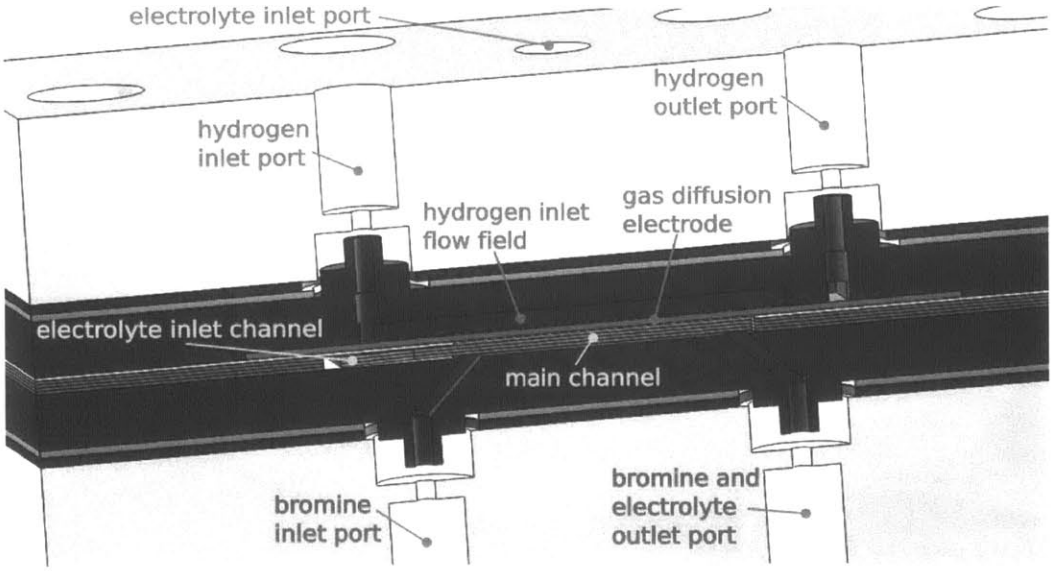

Figure 4-3: Interior view of the hydrogen bromine laminar flow battery stack assembly, sliced through the center of the stack along the centerline of the channel. O-rings, not pictured, create a seal between the posts on the current collectors and the recesses in the porting plates.

4.2.2 Materials

Bromine and hydrobromic acid are corrosive, and all parts of the cell that may contact these chemicals must be compatible with them. For this reason, other than the bolts, the cell is built out of carbon, glass, titanium, and fluoropolymer components.

4.2.3 Current collectors

The battery's current collectors are both machined from carbon-based materials. On the bromine side of the cell, the current collector is also the positive electrode and is made of graphite (McMaster-Carr, Robbinsville, NJ). Two channels for the injection and removal of the bromine stream are cut at 45-degree angles from the flow axis, and can be observed in Figure 4-3. This angled inlet and outlet connect inside the current collector to holes drilled straight into the current collector from the connectors to the porting plates.

The hydrogen-side current collector is made of a carbon composite. Less porous than graphite, it is better at containing the hydrogen gas. The electrolyte is injected and removed through holes machined through the current collector that line up with the beginning of the electrolyte channel in the electrolyte gaskets and the electrolyte inlet port in the porting plate. Hydrogen gas is introduced through the current collector into a channel that runs behind the recess in which the gas diffusion electrode sits. This hydrogen inlet flow field is labeled in

Figure 4-3. The hydrogen the flows outward through the gas diffusion electrode to reach two channels on either side of and parallel to the original channel, and is then removed through the current collector to the hydrogen outlet port. The connections to the porting plates are similar to those on the bromine current collector. Both current collectors are machined using a CNC mill (Roland DGA, Irvine, CA).

A titanium sheet backs the current collector, to reduce the electrical resistance from the active area to the tabs at the edges of the current collectors, where the cell is clipped to the potentiostat cables. This sheet is the same size as the current collector, with holes for bolts and porting.

On each side, between the titanium sheet and the current collector, a Viton rubber sheet (McMaster-Carr, Robbinsville, NJ) evens out irregularities to provide uniform compression in the cell, which is important for sealing and repeatable performance.

4.2.4 Hydrogen electrode

The hydrogen electrode is a carbon cloth gas diffusion electrode with 0.5 g/cm^2 platinum loading (FuelCellsEtc, College Station, TX). This material has a hydrophobic coating in addition to platinum loading, so it is suitable for creating a three-phase boundary between the hydrogen gas, the aqueous electrolyte, and the platinum catalyst on the electrolyte. It is cut to size using a cutting machine (Silhouette Cameo, Lehi, UT). The electrode fits into a recess machined in the hydrogen-side current collector. A fresh electrode is used with each cell build.

4.2.5 Channel gaskets

The channels through which the electrolyte and oxidant flow are made of polytetrafluoroethylene- (PTFE-) coated glass fiber cloth (Saint-Gobain, Malvern, PA). Each gasket is 180 μm thick. Like the hydrogen electrode, they are cut using the computer-controlled cutting machine. In the experiments described here, between one and four channel gaskets are stacked to achieve the desired channel height.

An additional thin sheet (13 μm) of perfluoroalkoxy alkane (PFA) (Saint-Gobain, Malvern, PA) between the channel gasket and the electrode and current collector blocks the electrolyte from contacting the electrode or current collector except in the intended active area and where necessary for porting. The active area is a 1.9 mm by 13 mm rectangle that falls between the oxidant inlet and the outlet.

Figure 4-4 is a photograph of the cell halfway disassembled, split through the stack of channel gaskets. On the bromine side, the channel gaskets are stacked on top of the current collector, titanium backing sheet, Viton gasket (not visible), and porting plate. On the hydrogen side, the PFA layer is visible where the channel appears slightly lighter outside the active area. Through the open channel, the hydrogen gas diffusion electrode is visible.

4.2.6 Porting plates

The porting plates are made of polyvinylidene fluoride (PVDF) (McMaster-Carr, Robbinsville, NJ), and, like the current collectors, are machined on the CNC mill. They seal to the connectors on the current collectors with a Viton O-ring (McMaster-Carr, Robbinsville, NJ), and, on the outside, port to the external tubing. PTFE tubing is used for chemical compatibility.

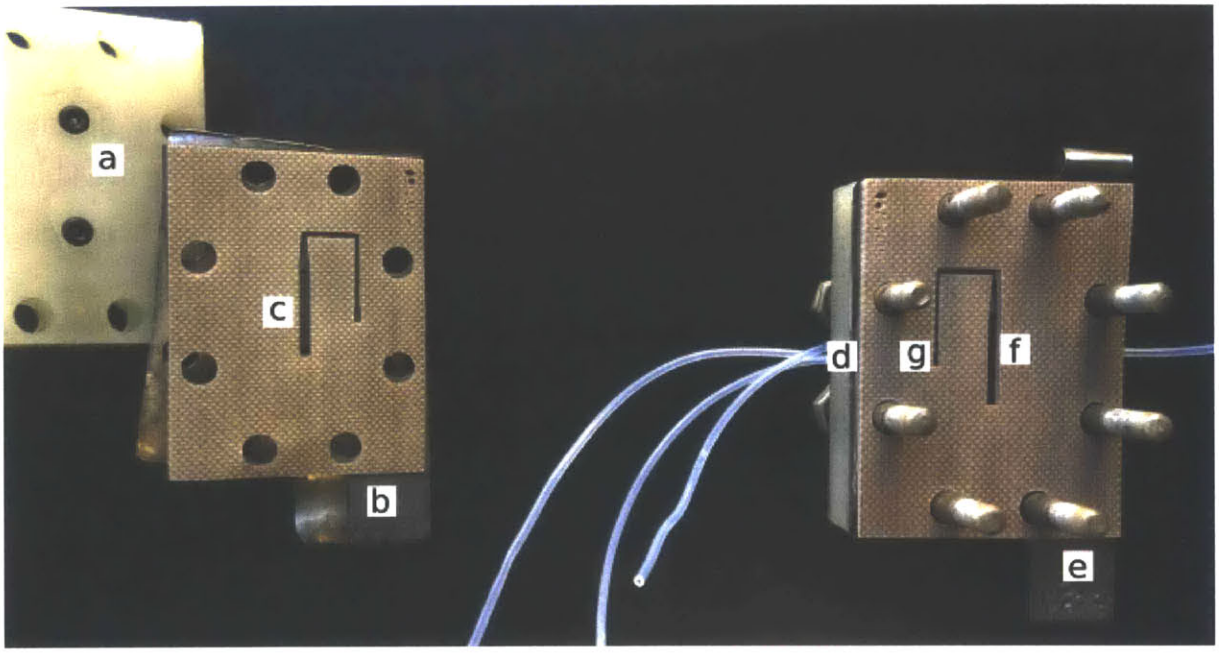

Figure 4-4: Photo of the interior of the battery prototype, split between two channel gaskets. On the left, the bromine porting plate (a) lies beneath the Viton gasket (not visible here), titanium sheet, and graphite current collector and bromine electrode (b). The electrode area is visible through the main channel (c), and the angled bromine inlet and outlet are visible at the top and bottom of the channel opening. On the right, the hydrogen and electrolyte porting plate (d) is stacked beneath the Viton gasket, titanium sheet (not visible here), carbon composite current collector (e), and channel gaskets through which the gas diffusion electrode is visible (f). The electrolyte is introduced into the main channel at (g). For scale, the dimensions of the channel gasket sheet are 4 cm by 6 cm.

4.2.7 Assembly

The components described above are stacked in the manner illustrated in Figure 4-2. The assembly is held together with eight 10-32 bolts, which are tightened with a torque wrench to 9 in-lb.

Chapter 5

Experimental Investigation of Effects of Mixing on Laminar Flow Battery Performance

5.1 Introduction

Experiments further support the idea developed in Chapter 3, that hydrodynamic focusing is particularly likely to contribute to mixing. This chapter presents the results from polarization curve experiments with the cell operating in single-pass discharge mode. The experiments using matched velocities match the predicted boundary layer limiting current density well for channel heights as low as 206 μm, which was not possible using hydrodynamic focusing.

5.2 Single-pass test setup and procedures

5.2.1 Fluid handling

For single-pass experiments, the two liquid streams were controlled using a syringe pump (Harvard Apparatus, Holliston, MA), and the hydrogen flow rate was maintained at 25 standard cubic centimeters per minute by a mass flow controller (Cole Parmer, Vernon Hills, IL), controlled by a Labview interface (National Instruments, Austin, TX).

The oxidant was 1 M bromine in 1 M hydrobromic acid, and the electrolyte was 1 M hydrobromic acid. The bromine solution was pumped from a 10-mL glass syringe (Hamilton, Reno, NV), and the hydrobromic acid solution was pumped from a 60-mL polypropylene syringe (Becton, Dickinson and Company, Franklin Lakes, NJ). They were connected to the cell using PTFE tubing (Cole Parmer, Vernon Hills, IL). Both lines of tubing were first filled with hydrobromic acid before the bromine was connected, in order to prevent bromine from reaching and degrading the anode during the first filling process.

The total flow rate of oxidant and electrolyte solutions was 1.15 mL/minute, which corresponds to a Reynolds number of 10 downstream of the junction. Before each experiment,

the cell was flushed with hydrobromic acid at 1.15 mL/minute for 30 seconds. After the flow rates were adjusted to the appropriate experimental conditions, the pressure measured above the cell was allowed to reach steady state before the polarization curve measurements were begun.

Figure 5-1 schematically illustrates the flows into and out of the cell. The oxidant and electrolyte were pumped into the cell separately, but were removed via a single outlet. Separating the oxidant and electrolyte downstream of the main channel will be necessary for operation as a battery, but was not attempted here, where the focus was on the behavior at the inlet.

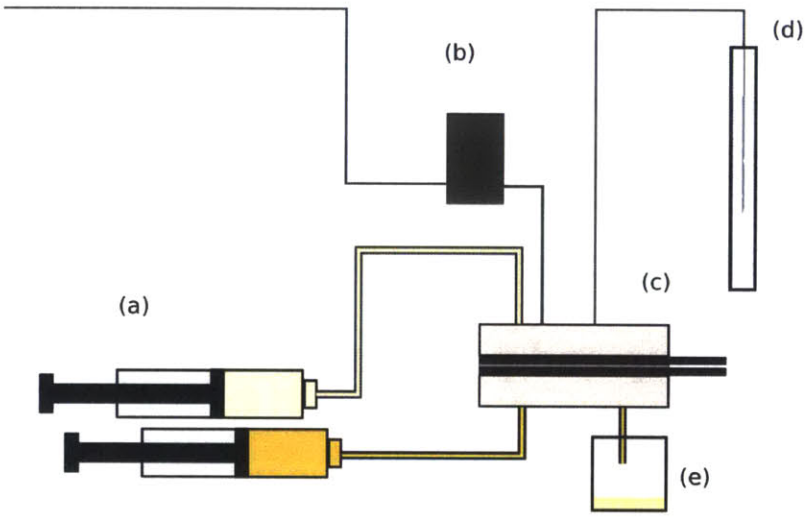

Figure 5-1: Schematic of experimental setup. In the single-pass setup, the flow of oxidant and electrolyte are controlled by a syringe pump (a), and the flow of hydrogen, by a mass flow controller (b). The cell stack assembly is (c). The hydrogen is bubbled out into a cylinder of water (d) in order to impose a small back pressure, and the oxidant and electrolyte exit to a waste container (e).

5.2.2 Polarization curve experimental procedure

Polarization curves were measured by applying steps of decreasing current while measuring the resulting cell voltage. In these experiments, each current density step was given a duration of 30 seconds. The voltage typically reached steady state within the first 10 seconds, so the voltage at each current step was taken to be the average of the last 20 seconds of voltage measurements. The experiment was stopped when the voltage dropped below 0 V for any period of time. Results are reported in terms of average current density, which is the current normalized to the active area. The electrochemical measurements were made using a Reference 3000 potentiostat (Gamry Instruments, Warminster, PA). The polarization curve procedure was programmed in Labview (National Instruments, Austin, TX).

Polarization curves with sudden drops in the middle of a current step were discarded--this behavior can indicate the intrusion of gas bubbles in the channel, obstructing flow. This can be a challenge especially at the smaller channel heights, because it can cause the experiment stop running before reaching the diffusion-limited current.

5.2.3 Determination of limiting current

The expected polarization curve behavior is that activation losses are low, so that at low currents, ohmic losses dominate, until the potential drops rapidly as it approaches some limiting current. As long as the ohmic losses are not so large that they cause the cell to drop to 0 V before reaching limiting current, and assuming that there is no overlimiting current mechanism that presents itself first, the cell potential should drop to 0 V near the limiting current.

From the polarization curve, the limiting current density was approximated as the sum of the last current density at which a full step's worth of measurements may be taken before dropping below 0 V and half the current density step (Figure 5-2). This should be within half of a current density step of the actual 0-V intercept, which was taken as a proxy for limiting current.

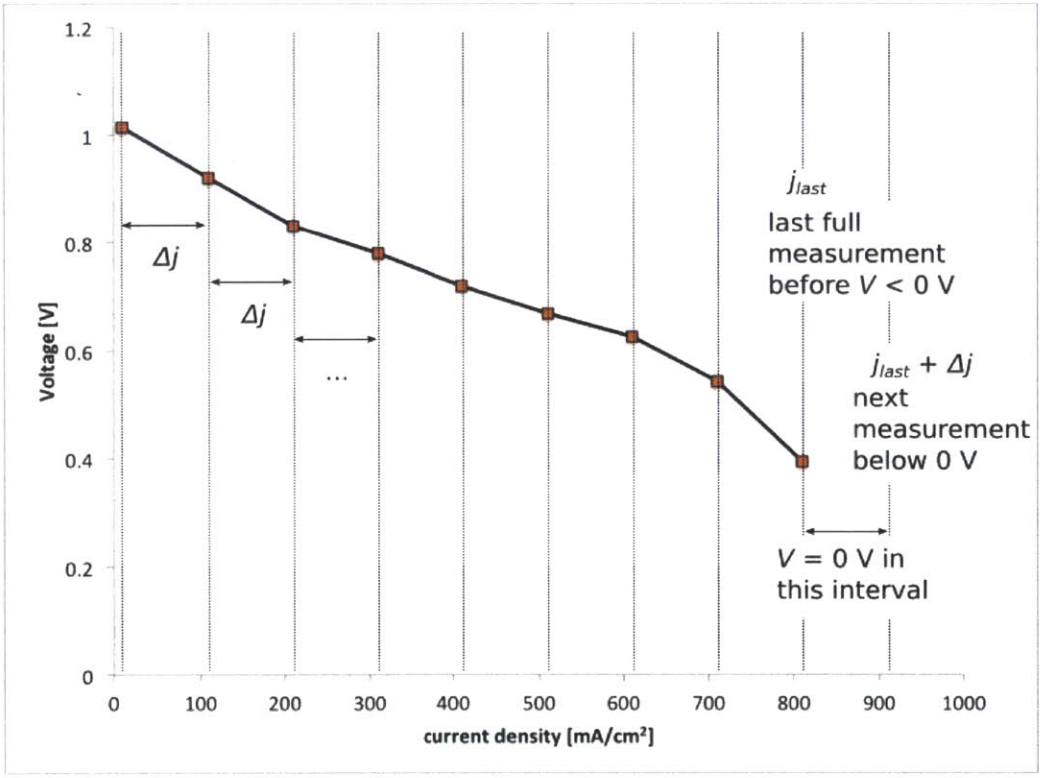

Figure 5-2: The $V = 0$ V intercept occurs at $j_{last} + \frac{\Delta j}{2}$ with an error of $\pm\frac{\Delta j}{2}$

5.3 Experimental results

5.3.1 Polarization curve results

The primary trend observed in the polatization curve results is that, moving from hydrodynamic focusing, to matched inlet flow rate, to matched inlet velocity, the limiting current increases up to a point, and the results become more consistent with each other.

With a Reynolds number of 10 and a 10:1 electrolyte-oxidant flow rate ratio, the cell obeyed limiting current at a channel height of 746 μm (Figure 5-3), but not at a channel height of 566 μm (Figure 5-4). In the previous experiments by Braff et al., a similar difference was found with channel heights of 800 μm and 600 μm.

Figure 5-3 shows the polarization curve measurements for the 746-μm channel height build. The sudden drop of voltage associated with approaching limiting current is evident. The polarization curves for the three trials at matched inlet velocities and those at matched flow rates reached the highest current density before dropping below 0 V, and the curves at matched velocities appear the most repeatable.

The resistance of the cell at lower current densities is higher than predicted in Chapter 2. This resistance is observed at all channel heights. While this extra resistance affects the cell's power output significantly, it should not affect the limiting current.

Figure 5-4 shows results for the same set of inlet flow conditions in the 566-μm channel-height build. Here, the matched flow rate and matched velocity cases are so consistent with each other that the data for the matched flow rates are nearly obscured by the data for the matched velocities. Again the 10:1 flow rate ratio case is the least repeatable and reaches the lowest current density before falling below a potential of 0 V.

Figure 5-5 and Figure 5-6 show the polarization curve results for the 386-μm and 206-μm channel height cases, respectively. These results also show higher limiting currents achieved for matched flow rates and velocities. These two figures also show that a drop in open circuit potential is observed in the same polarization curves that significantly fall short of the highest limiting current density observed for that build. As discussed in Chapter 2, a drop in open circuit potential is expected if mixing decreases the bulk concentration of the oxidant.

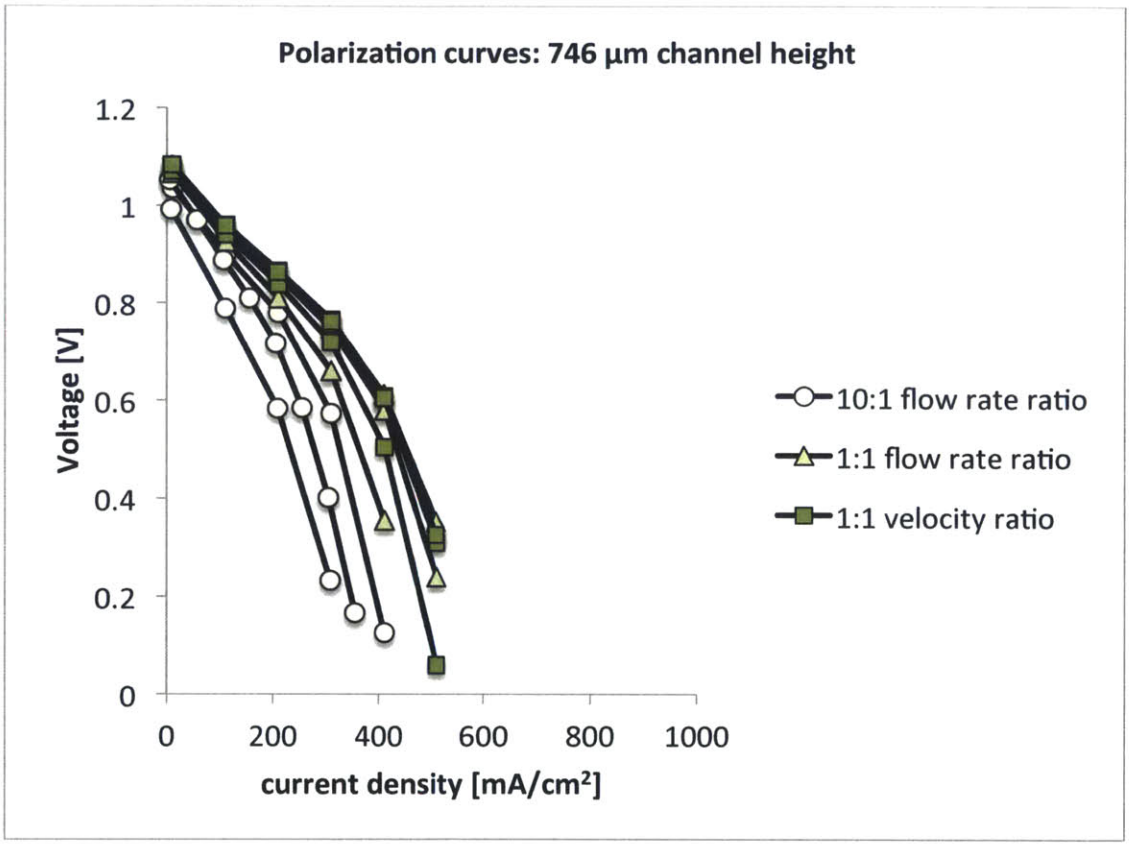

Figure 5-3: Polarization curves for battery with 746-µm channel height. Three trials are shown at each of three inlet flow rate conditions. In all cases, Reynolds number is 10 in the main channel downstream of the junction.

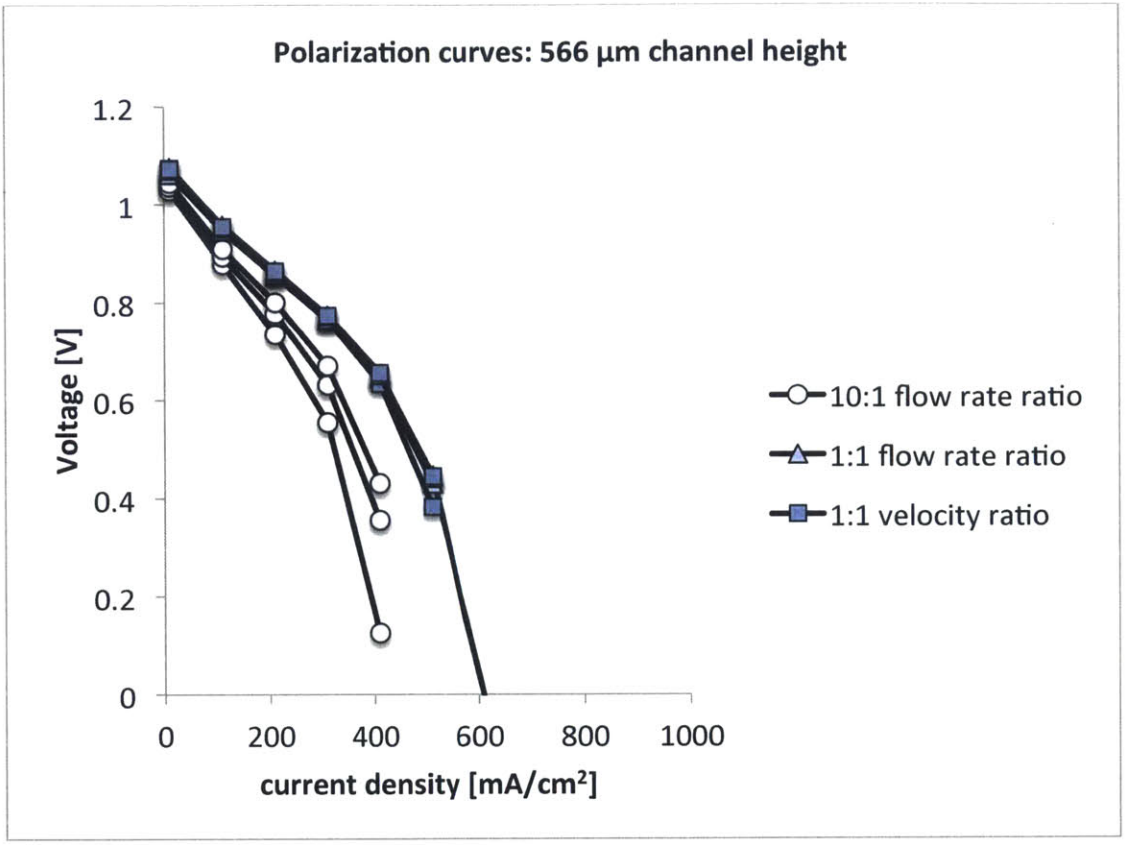

Figure 5-4: Polarization curves for battery with 566-µm channel height. Three trials are shown at each of three inlet flow rate conditions. In all cases, Reynolds number is 10 in the main channel downstream of the junction.

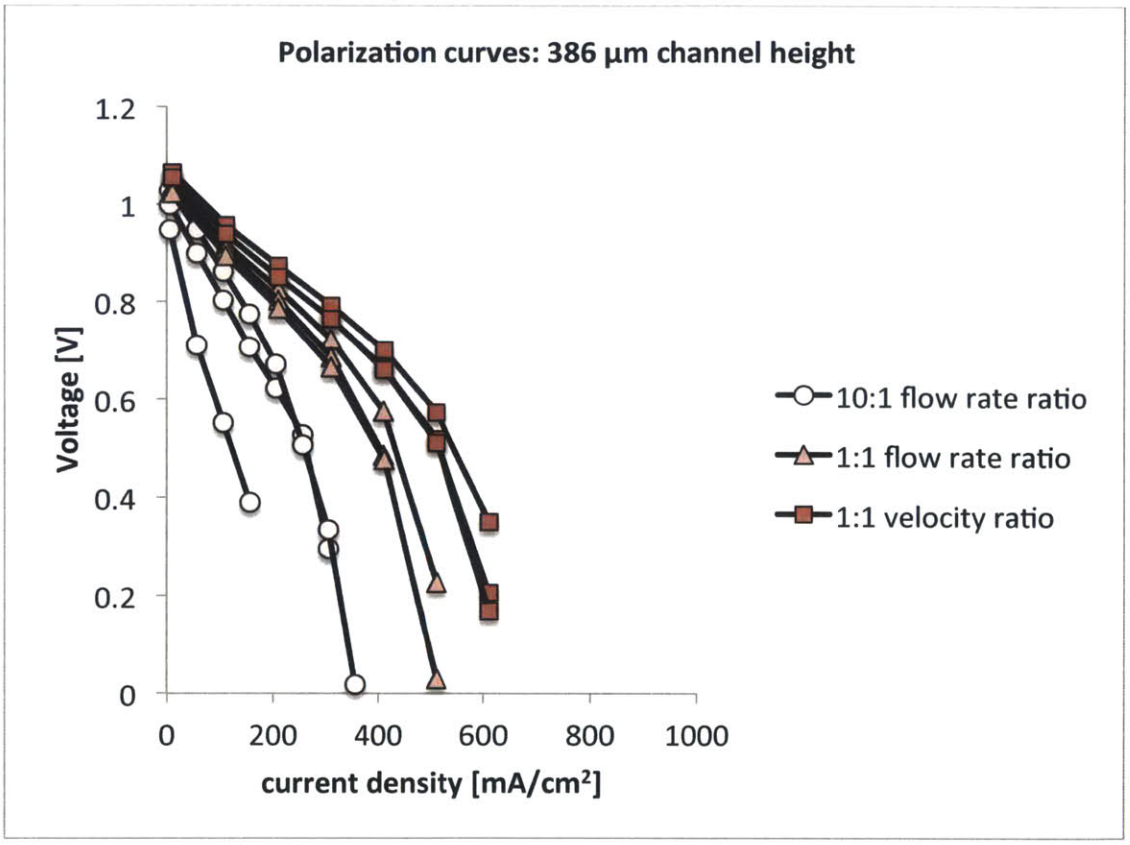

Figure 5-5: Polarization curves for battery with 386-µm channel height. Three trials are shown at each of three inlet flow rate conditions. In all cases, Reynolds number is 10 in the main channel downstream of the junction.

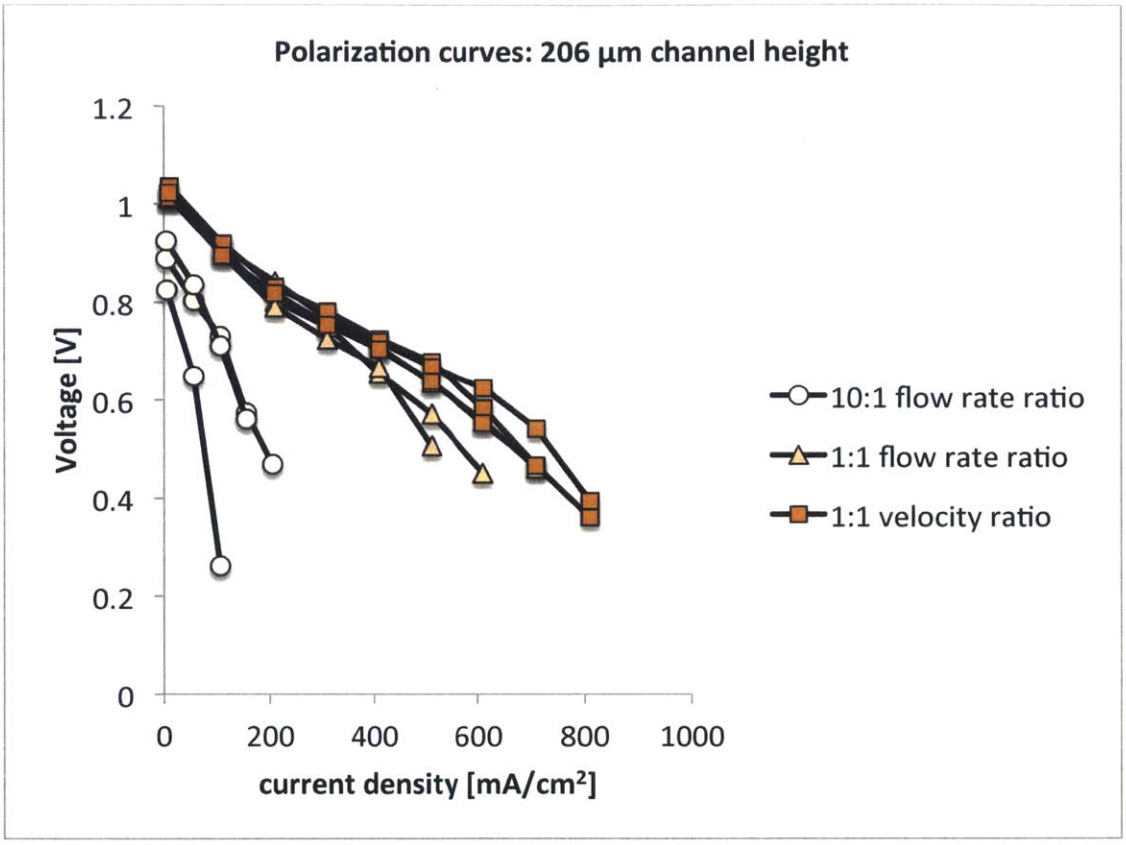

Figure 5-6: Polarization curves for battery with 206-µm channel height. Three trials are shown at each of three inlet flow rate conditions. In all cases, Reynolds number is 10 in the main channel downstream of the junction.

5.3.2 Limiting current behavior

These experiments show that, although the limiting current fails to increase with decreasing channel heights as predicted when flow focusing is employed, the limiting current behavior is consistent with predictions when velocities or flow rates are matched at the two inlets.

The previous work discussed above, which employed flow focusing, had shown that, counter to predictions, the limiting current decreased with decreasing channel height.[22] This same trend is shown in Figure 5-7, which is at the same flow rate conditions as the previous work, with a 10:1 electrolyte-to-oxidant flow rate ratio. The solid black line shows the analytical boundary-layer limiting current for the "bulk" concentrations consistent with no mixing; the dashed black line, for concentrations consistent with complete mixing at the given flow rates. The behavior of the measured results in the smaller channels is consistent with some mixing. Given the uncertainty associated with the small number of experiments and the methodology, it is impossible to specify the degree of mixing. However, this observation, in combination with the evidence from the open circuit potential for the same two cases discussed above, supports the conclusion that mixing is occurring at the two smallest channel heights when the electrolyte-oxidant flow rate ratio is 10:1.

When flow rates are matched, however, a different trend begins to emerge, which is more consistent with the predictions from the boundary layer analysis. These results are shown in Figure 5-8. Here, the "fully mixed" limiting current has increased from the previous case, because, when flow rates are matched, there is less electrolyte to dilute the oxidant in this worst-case mixing scenario. Because of this, and because of the uncertainty of the measurements, these results are somewhat inconclusive in the case of the 206-μm channel. Matching flow rates may prevent mixing. Further experiments with more trials and smaller current steps in the polarization curve procedure could provide stronger evidence.

The results for the case of matched average velocities in oxidant and electrolyte inlets upstream of the junction are shown in Figure 5-9. More than in any other case, here at small channel heights, the measurements agree well with the predicted limiting current.

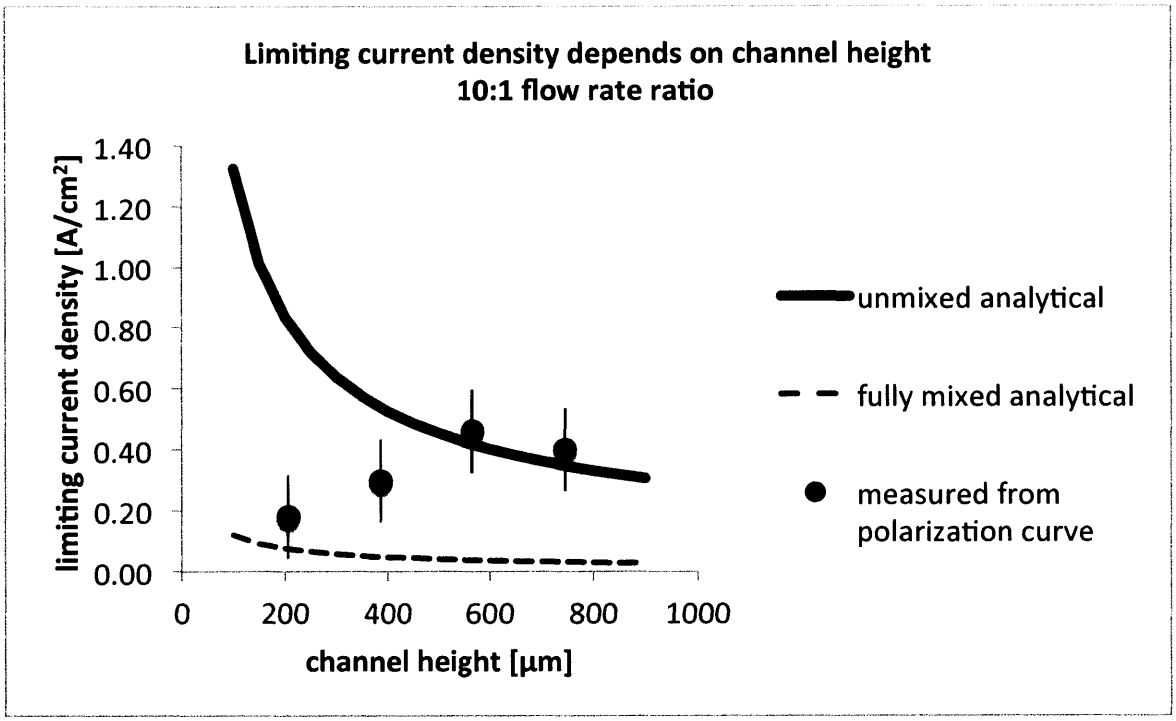

Figure 5-7: Measured limiting current density plotted versus channel height with an electrolyte-to-oxidant flow rate ratio of 10:1. Each experiment has a Reynolds number of 10 in the main channel. N=3.

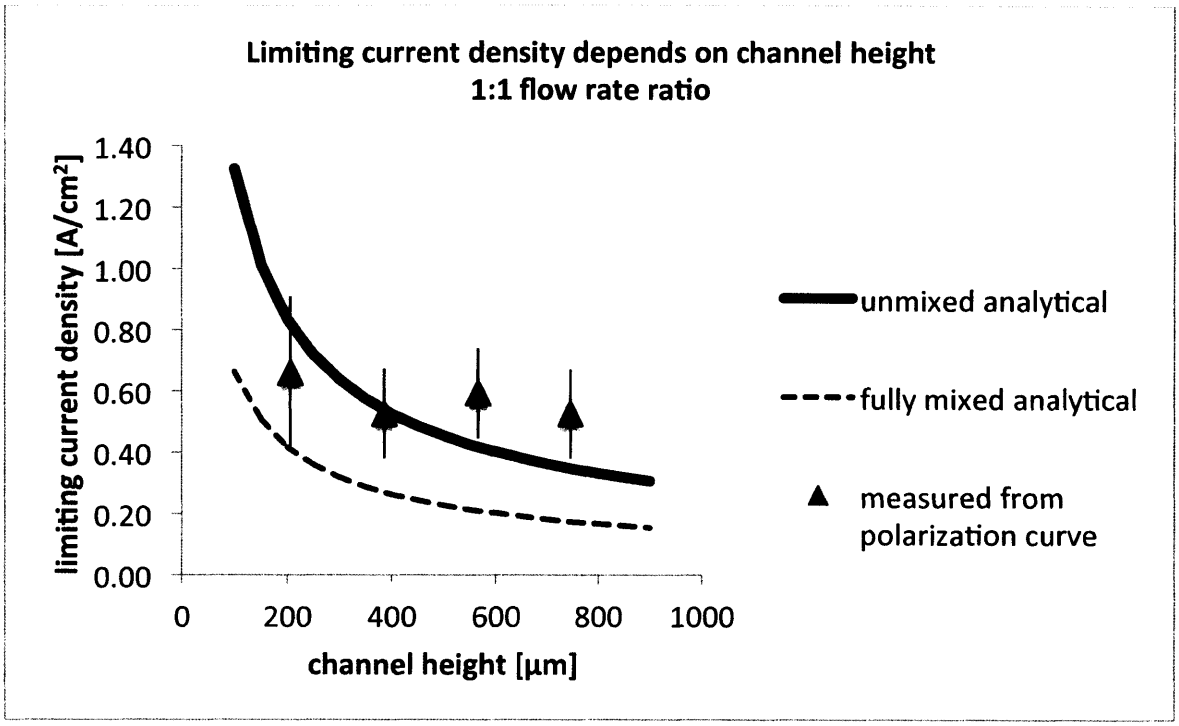

Figure 5-8: Measured limiting current density plotted versus channel height with an electrolyte-to-oxidant flow rate ratio of 1:1. Each experiment has a Reynolds number of 10 in the main channel. N=3.

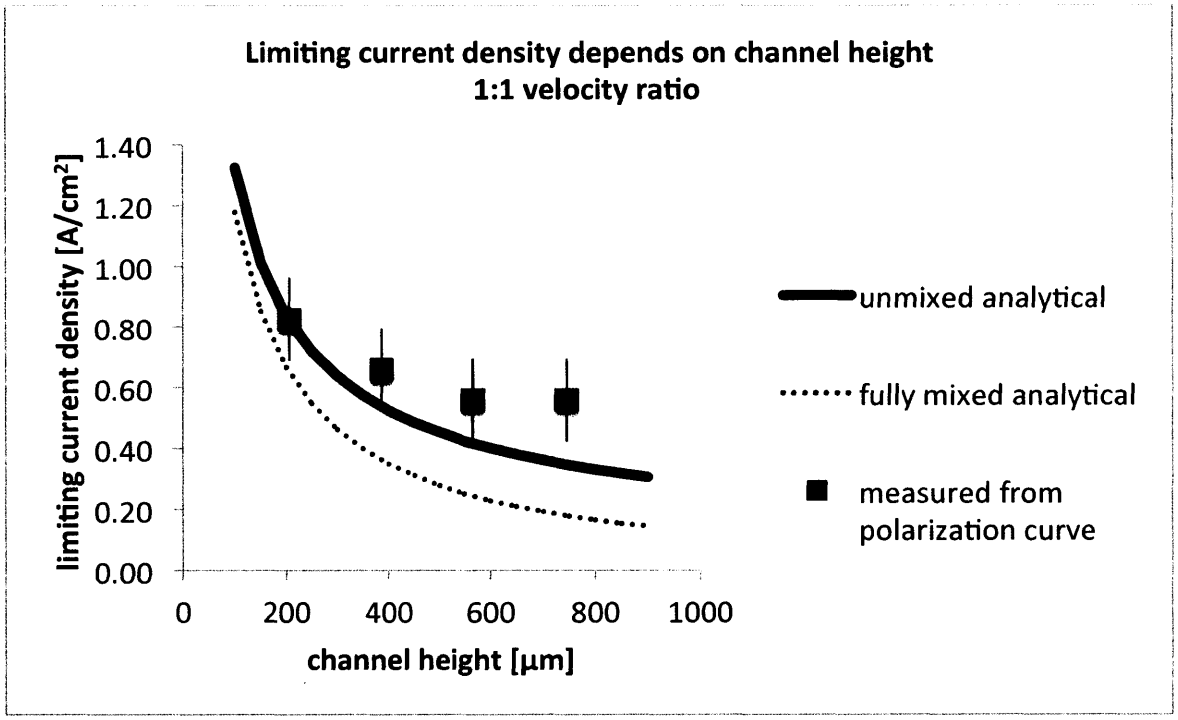

Figure 5-9: Measured limiting current density plotted versus channel height with an electrolyte-to-oxidant velocity ratio of 1:1. Each experiment has a Reynolds number of 10 in the main channel. N=3.

Chapter 6

Conclusions and Future Work

6.1 Role of inertial mixing

The coinciding evidence of recirculating flows in two dimensional flow simulations and drastic drops in observed limiting current in polarization curve experiments when hydrodynamic focusing is employed at small channel heights supports the hypothesis that inertial flow at the inlet is associated with poor battery performance.

These experiments also found it possible, for the first time with the hydrogen bromine laminar flow battery, to experimentally reach the limiting current density predicted by boundary layer analysis at channel heights less than or equal to 600 μm, at least when matching velocity ratios. This suggests a path forward, in which the next iteration of the hydrogen bromine laminar flow battery architecture considers how the oxidant and electrolyte streams may be brought together as symmetrically as possible.

6.2 Power density

In the original work with the hydrogen bromine laminar flow battery, the failure to reach higher limiting currents in smaller channels was the limiting factor in increasing the power density of the cell. Here, that limitation is lifted. Unfortunately, there is a new limitation: the extra resistance mentioned in Section 5.3.1. These losses are associated with the bromine reaction at the electrode, and were not observed previously. With these extra losses, a maximum power density of 0.385 W/cm^2 was observed in one of the 206-μm, matched-velocity experiments. If these losses are eliminated, the demonstrated improvements in limiting current density promise to allow the planar-electrode hydrogen bromine laminar flow battery to reach its highest power density yet.

6.3 Next steps

A pressing next step is to understand and eliminate the extra resistance described above. Electrochemical impedance spectroscopy experiments have traced the resistance to the cathode,

but more work is needed to understand what is happening. Once this is understood, the results on mixing in the cell presented here will inform the design of new experiments without hydrodynamic focusing, to investigate the maximum power density attainable with the planar-electrode hydrogen bromine laminar flow battery.

References

(1) Goodenough, J. B.; Park, K.-S. The Li-Ion Rechargeable Battery: A Perspective. *J. Am. Chem. Soc.* **2013**, *135*, 1167–1176.

(2) Yang, Z.; Zhang, J.; Kintner-Meyer, M. C. W.; Lu, X.; Choi, D.; Lemmon, J. P.; Liu, J. Electrochemical Energy Storage for Green Grid. *Chem. Rev.* **2011**, *111*, 3577–3613.

(3) Dunn, B.; Kamath, H.; Tarascon, J.-M. Electrical Energy Storage for the Grid: A Battery of Choices. *Science* **2011**, *334*, 928–935.

(4) Weber, A. Z.; Mench, M. M.; Meyers, J. P.; Ross, P. N.; Gostick, J. T.; Liu, Q. Redox Flow Batteries: A Review. *J. Appl. Electrochem.* **2011**, *41*, 1137–1164.

(5) Rehman, S.; Al-Hadhrami, L. M.; Alam, M. M. Pumped Hydro Energy Storage System: A Technological Review. *Renew. Sustain. Energy Rev.* **2015**, *44*, 586–598.

(6) Zakeri, B.; Syri, S. Electrical Energy Storage Systems: A Comparative Life Cycle Cost Analysis. *Renew. Sustain. Energy Rev.* **2015**, *42*, 569–596.

(7) Ponce de León, C.; Frías-Ferrer, A.; González-García, J.; Szánto, D. A.; Walsh, F. C. Redox Flow Cells for Energy Conversion. *J. Power Sources* **2006**, *160*, 716–732.

(8) Skyllas-Kazacos, M.; Kazacos, G.; Poon, G.; Verseema, H. Recent Advances with UNSW Vanadium-Based Redox Flow Batteries. *Int. J. Energy Res.* **2010**, *34*, 182–189.

(9) Skyllas-Kazacos, M.; Kasherman, D.; Hong, D. R.; Kazacos, M. Characteristics and Performance of 1 kW UNSW Vanadium Redox Battery. *J. Power Sources* **1991**, *35*, 399–404.

(10) Skyllas-Kazacos, M.; Chakrabarti, M. H.; Hajimolana, S. A.; Mjalli, F. S.; Saleem, M. Progress in Flow Battery Research and Development. *J. Electrochem. Soc.* **2011**, *158*, R55–R79.

(11) Cunha, Á.; Martins, J.; Rodrigues, N.; Brito, F. P. Vanadium Redox Flow Batteries: A Technology Review. *Int. J. Energy Res.* **2015**, *39*, 889–918.

(12) Ferrigno, R.; Stroock, A. D.; Clark, T. D.; Mayer, M.; Whitesides, G. M. Membraneless Vanadium Redox Fuel Cell Using Laminar Flow. *J. Am. Chem. Soc.* **2002**, *124*, 12930–12931.

(13) Yeo, R. S.; Chin, D.-T. A Hydrogen-Bromine Cell for Energy Storage Applications. *J. Electrochem. Soc.* **1980**, *127*, 549–555.

(14) Kosek, J. A.; Laconti, A. B. Advanced Hydrogen Electrode for a Hydrogen-Bromine Battery. *J. Power Sources* **1988**, *22*, 293–300.

(15) Cho, K. T.; Albertus, P.; Battaglia, V.; Kojic, A.; Srinivasan, V.; Weber, A. Z. Optimization and Analysis of High-Power Hydrogen/Bromine-Flow Batteries for Grid-Scale Energy Storage. *Energy Technol.* **2013**, *1*, 596–608.

(16) Cho, K. T.; Tucker, M. C.; Ding, M.; Ridgway, P.; Battaglia, V. S.; Srinivasan, V.; Weber, A. Z. Cyclic Performance Analysis of Hydrogen/Bromine Flow Batteries for Grid-Scale Energy Storage. *ChemPlusChem* **2015**, *80*, 402–411.

(17) Braff, W. A.; Bazant, M. Z.; Buie, C. R. Membrane-Less Hydrogen Bromine Flow Battery. *Nat. Commun.* **2013**, *4*.

(18) U.S. Geological Survey. *Mineral Commodity Summaries 2015*; U.S. Geological Survey; p. 196.

(19) Braff, W. A.; Buie, C. R.; Bazant, M. Z. Boundary Layer Analysis of Membraneless Electrochemical Cells. *J. Electrochem. Soc.* **2013**, *160*, A2056–A2063.

(20) Singh, N.; McFarland, E. W. Levelized Cost of Energy and Sensitivity Analysis for the Hydrogen–bromine Flow Battery. *J. Power Sources* **2015**, *288*, 187–198.
(21) Braff, W. A. Membraneless Hydrogen Bromine Laminar Flow Battery for Large-Scale Energy Storage, Massachusetts Institute of Technology: Cambridge, MA, 2014.
(22) Braff, W. A.; Bazant, M. Z.; Buie, C. R. Inertial Effects on the Generation of Co-Laminar Flows. *J. Fluid Mech.* **2015**, *767*, 85–94.
(23) *CRC Handbook of Chemistry and Physics*; Haynes, W. M., Ed.; 96th ed.; CRC Press, 2015.
(24) Kreutzer, H.; Yarlagadda, V.; Nguyen, T. V. Performance Evaluation of a Regenerative Hydrogen-Bromine Fuel Cell. *J. Electrochem. Soc.* **2012**, *159*, F331–F337.
(25) Da Mota, N.; Finkelstein, D. A.; Kirtland, J. D.; Rodriguez, C. A.; Stroock, A. D.; Abruña, H. D. Membraneless, Room-Temperature, Direct Borohydride/Cerium Fuel Cell with Power Density of Over 0.25 W/cm2. *J. Am. Chem. Soc.* **2012**, *134*, 6076–6079.
(26) Di Carlo, D. Inertial Microfluidics. *Lab. Chip* **2009**, *9*, 3038–3046.
(27) Jayashree, R. S.; Yoon, S. K.; Brushett, F. R.; Lopez-Montesinos, P. O.; Natarajan, D.; Markoski, L. J.; Kenis, P. J. A. On the Performance of Membraneless Laminar Flow-Based Fuel Cells. *J. Power Sources* **2010**, *195*, 3569–3578.
(28) Nasir, M.; Mott, D. R.; Kennedy, M. J.; Golden, J. P.; Ligler, F. S. Parameters Affecting the Shape of a Hydrodynamically Focused Stream. *Microfluid. Nanofluidics* **2011**, *11*, 119–128.
(29) Dreher, S.; Kockmann, N.; Woias, P. Characterization of Laminar Transient Flow Regimes and Mixing in T-Shaped Micromixers. *Heat Transf. Eng.* **2009**, *30*, 91–100.
(30) Kockmann, N.; Föll, C.; Woias, P. Flow Regimes and Mass Transfer Characteristics in Static Micromixers. In; 2003; Vol. 4982, pp. 319–329.
(31) Wong, S. H.; Ward, M. C. L.; Wharton, C. W. Micro T-Mixer as a Rapid Mixing Micromixer. *Sens. Actuators B Chem.* **2004**, *100*, 359–379.
(32) Choban, E. R.; Markoski, L. J.; Wieckowski, A.; Kenis, P. J. A. Microfluidic Fuel Cell Based on Laminar Flow. *J. Power Sources* **2004**, *128*, 54–60.
(33) Cohen, J. L.; Westly, D. A.; Pechenik, A.; Abruña, H. D. Fabrication and Preliminary Testing of a Planar Membraneless Microchannel Fuel Cell. *J. Power Sources* **2005**, *139*, 96–105.
(34) Jayashree, R. S.; Gancs, L.; Choban, E. R.; Primak, A.; Natarajan, D.; Markoski, L. J.; Kenis, P. J. A. Air-Breathing Laminar Flow-Based Microfluidic Fuel Cell. *J. Am. Chem. Soc.* **2005**, *127*, 16758–16759.
(35) Kjeang, E.; Proctor, B. T.; Brolo, A. G.; Harrington, D. A.; Djilali, N.; Sinton, D. High-Performance Microfluidic Vanadium Redox Fuel Cell. *Electrochimica Acta* **2007**, *52*, 4942–4946.
(36) Lee, J. W.; Kjeang, E. Nanofluidic Fuel Cell. *J. Power Sources* **2013**, *242*, 472–477.
(37) Lee, J. W.; Goulet, M.-A.; Kjeang, E. Microfluidic Redox Battery. *Lab. Chip* **2013**, *13*, 2504–2507.
(38) Goulet, M.-A.; Kjeang, E. Reactant Recirculation in Electrochemical Co-Laminar Flow Cells. *Electrochimica Acta* **2014**, *140*, 217–224.